Solution Structure of the Osteogenic 1−31 Fragment of the Human Parathyroid Hormone†

Zhigang Chen,‡ Ping Xu,‡ Jean-René Barbier,§ Gordon Willick,§ and Feng Ni*,‡

Biomolecular NMR Laboratory and the Montréal Joint Centre for Structural Biology, Biotechnology Research Institute, National Research Council of Canada, Montréal, Québec, Canada H4P 2R2 and the Institute for Biological Sciences, National Research Council of Canada, Ottawa, Ontario, Canada K1A 0R6

Received April 18, 2000; Revised Manuscript Received August 8, 2000

ABSTRACT: The solution conformations of a selectively osteogenic 1−31 fragment of the human parathyroid hormone (hPTH), hPTH(1−31)NH_2, have been characterized by use of very high field NMR spectroscopy at 800 MHz. The combination of the CαH proton and $^{13}C\alpha$ chemical shifts, $^3J_{NH\alpha}$ coupling constants, NH proton temperature coefficients, and backbone NOEs reveals that the hPTH(1−31)NH_2 peptide has well-formed helical structures localized in two distinct segments of the polypeptide backbone. There are also many characteristic NOEs defining specific side-chain/backbone and side-chain/side-chain contacts within both helical structures. The solution structure of hPTH(1−31)NH_2 contains a short N-terminal helical segment for residues 3−11, including the helix capping residues 3 and 11 and a long C-terminal helix for residues 16−30. The two helical structures are reinforced by well-defined capping motifs and side-chain packing interactions within and at both ends of these helices. On one face of the C-terminal helix, there are side-chain pairs of Glu22−Arg25, Glu22−Lys26, and Arg25−Gln29 that can form ion-pair and/or hydrogen bonding interactions. On the opposite face of this helix, there are characteristic hydrophobic interactions involving the aromatic side chain of Trp23 packing against the aliphatic side chains of Leu15, Leu24, Lys27, and Leu28. There is also a linear array of hydrophobic residues from Val2, to Leu7, to Leu11 and continuing on to residues His14 and Leu15 in the hinge region and to Trp23 in the C-terminal helix. Capping and hydrophobic interactions at the end of the N-terminal and at the beginning of the C-terminal helix appear to consolidate the helical structures into a V-shaped overall conformation for at least the folded population of the hPTH(1−31)NH_2 peptide. Stabilization of well-folded conformations in this linear 1−31 peptide fragment and possibly other analogues of human PTH may have a significant impact on the biological activities of the PTH peptides in general and specifically for the osteogenic/anabolic activities of bone-building PTH analogues.

Parathyroid hormone (PTH)[1] is the key hormone for the regulation of calcium levels in animal serum. PTH functions principally through its actions on the seven transmembrane G-protein-linked receptors in kidney, bone, and intestinal cells. The PTH−receptor interactions activate two distinct signaling pathways, one involving the adenylyl cyclase (AC) and AC-associated protein kinase A and another involving the phospholipase Cβ and the associated protein kinase C (PKC) (*1*−*3*). Virtually all the functions of human PTH (hPTH) are encoded within the N-terminal 34 amino acid residues of the 84-residue full-length protein, as the 1−34 peptide fragment, or hPTH(1−34), is fully active (*4*) and displays both AC stimulation and PKC activities (*5*). AC activation requires at least the N-terminal 28 residues of PTH (*6*, *7*), whereas PKC activation appears to require a much shorter sequence of residues 29−32, at least in rat osteosarcoma (ROS) cells (*8*−*11*). Very interestingly, a C-terminally truncated analogue of hPTH(1−34), or hPTH(1−31)NH_2, has only the AC-stimulating activity in ROS cells (*10*) but shows full anabolic potency in the ovariectomized rat model of osteoporosis (*12*, *13*). In addition, hPTH(1−31)NH_2 was found to have comparable AC-stimulating activity to hPTH(1−34), but it did not cause hypercalcemia, thus appearing not to cause rapid bone resorption in humans (*14*) as can result from hPTH(1−34) treatment. As such, selectively osteogenic analogues of human PTH may represent a new generation of therapeutics for the treatment of osteoporosis (*2*, *15*).

To achieve a better understanding of the functional activities of PTH, the conformations of full-length PTH and the bioactive peptide fragments hPTH(1−34) and hPTH(1−37) have been studied under a variety of solution conditions. Circular dichroism (CD) spectra, acquired at neutral pH and

† This work was made possible by use of an 800-MHz NMR facility, which is funded by the National Research Council of Canada, the parent institution of both the Biotechnology Research Institute and the Institute for Biological Sciences. This is NRCC publication number 42960.

* To whom correspondence should be addressed: E-mail: Feng.Ni@nrc.ca; phone: (514) 496-6729; fax: (514) 496-5143.

‡ Biotechnology Research Institute, National Research Council of Canada.

§ Institute for Biological Sciences, National Research Council of Canada.

[1] Abbreviations: PTH, parathyroid hormone; hPTH, human parathyroid hormone; AC, adenylyl cyclase; PKC, protein kinase C; ROS, rat osteosarcoma; CD, circular dichroism; NMR, nuclear magnetic resonance; NOE, nuclear Overhauser effect; HSQC, heteronuclear single quantum correlation; NOESY, nuclear Overhauser effect spectroscopy; TOCSY, total correlation spectroscopy; ROESY, rotating frame Overhauser effect spectroscopy; DQF-COSY, double quantum filtered correlation spectroscopy; TPPI, time-proportional phase incrementation; DSS, 2,2-dimethyl-silapentane-5-sulfonic acid; DG, distance geometry; SA, simulated annealing.

10.1021/bi000882e CCC: $19.00 Published 2000 by the American Chemical Society
Published on Web 09/28/2000

moderate ionic strength, indicated the presence of helical conformations in PTH and selected fragments (*7*, *16*). As with many polypeptide hormones, the full-length PTH does not have a well-defined tertiary structure in aqueous solution at physiological pH and ionic strength (*17*, *18*). NMR studies of hPTH(1−34) and hPTH(1−37) indicate the presence of a helical structure between residues 17 and 29 in the presence of varying levels of trifluoroethanol (TFE), in acidic media, and/or in the presence of micelles, while residues 3−12 show some population of helical conformations (*19*−*23*). The hPTH(1−37) peptide was shown to have a better defined structure with some degree of tertiary interactions in an aqueous solution at close to neutral pH and with a moderate ionic strength (*24*). The latest NMR data showed that both the hPTH(1−34) and hPTH(1−37) peptides have two loosely connected structural subdomains, one of residues 15−29 with a well-defined helical structure and the second of residues 1−12 with a more flexible conformation (*25*, *26*).

In our current work, we started an NMR investigation of the conformational details of the osteogenic analogues of human PTH to define the structural determinants responsible for the anabolic/osteogenic activity. Our work was greatly facilitated by the finding that the linear hPTH(1−31)NH_2 is at least as well structured as the longer hPTH(1−34) or hPTH(1−37) fragments, judged by circular dichroism data (*7*) and by the high-quality proton NMR spectra. Limited resonance dispersion intrinsic to partially folded peptides such as the PTH fragments was greatly improved by use of the recently available very high field NMR at 800 MHz. Increased sensitivity with the recently developed NMR pulse sequences (*27*, *28*) also made it possible to characterize the solution conformations of bioactive peptides in much greater detail and under physiologically relevant conditions, namely, at much lower concentrations and at neutral pH with proper ionic strength (*29*, *30*). In this paper, we describe the high-resolution solution structure of the selectively osteogenic hPTH(1−31)NH_2 peptide and compare it with those for longer PTH fragments. We intend to assess in detail the conformational effects of removing three to six C-terminal residues from hPTH(1−34) or hPTH(1−37) and to determine whether it is conformational alterations that may render the shorter hPTH(1−31)NH_2 peptide as a selectively osteogenic or anabolic agent for the growth of bone.

MATERIALS AND METHODS

Preparation of NMR Samples. The peptide hPTH(1−31)-NH_2 was synthesized and purified as described previously (*31*). Weighed amounts (1−2 mg) of the purified peptide were first dissolved in 200−400 microliters (μL) of water containing both H_2O and D_2O. To the solutions of the peptides thus obtained were added solids of the NaCl salt in amounts appropriate for a final concentration of 300 mM in NaCl. The pH values of the peptide samples were adjusted by the addition of an equal volume of an aqueous solution that was 50 mM in sodium phosphate and 0.4 mM in EDTA at pH 7.2. The final solutions contained between 2 and 5 mg/mL (or 0.6−1.56 mM) of the peptides in 25 mM of sodium phosphate, 0.2 mM of EDTA, 300 mM of NaCl, and 10% of D_2O with a pH value of 6.8. Under these solution conditions, the circular dichroism (CD) spectra of the hPTH-(1−31)NH_2 peptide showed the same characteristic helical signature at peptide concentrations of 12.8 and 115 μM. Proton resonances were also relatively sharp and remained the same at increasing dilutions of the NMR samples down to 30 μM. NOESY spectra contained similar cross-peaks for the peptide samples at the higher concentration of 1.2 mM and at a low concentration of 0.2 mM. Taken together, both CD and NMR experiments indicate the absence of peptide aggregation and/or conformational changes under the solution conditions used for NMR studies.

NMR Experiments. The NMR experiments were carried out on a Bruker Avance-500 or an Avance-800 NMR spectrometer at a temperature range of 278 to 298 K. All two-dimensional spectra were acquired in phase-sensitive mode using time-proportional phase incrementation (TPPI) for quadrature detection in the t_1 dimension (*32*). The two-dimensional NMR experiments included NOESY with flip back of the water proton resonance, or water-flipback NOESY (*28*, *33*), F1-inphase COSY (Xu and Ni, unpublished data), ROESY (*34*), and water-flipback TOCSY implemented using the TOWNY-16 spin-lock sequence (*27*, *35*). The suppression of the water proton resonance was achieved for all two-dimensional NMR experiments using the WATER-GATE method implemented through the 3-9-19 pulse train (*36*, *37*). Mixing times of 30 and 70 ms were used for the TOCSY experiments, 100, 150, 200, and 250 ms were used for the NOESY, and 200 ms was used for the ROESY spectra. In the ROESY experiments, the spin-lock field was delivered by continuous wave irradiation with compensation of off-resonance effects (*34*). The typical spectral widths were 6024 Hz at 500 MHz and 9980 Hz at 800 MHz in both spectral dimensions. Free induction decays were acquired with 2K complex data points for the TOCSY, ROESY, and NOESY data sets and with 4K complex data points for the F1-inphase COSY experiments. A total of 400 t_1 increments were collected for ROESY, NOESY, and TOCSY data and 256 for F1-inphase DQF-COSY data sets. Sine modulation was used along the t_1 dimension, with the initial t_1 delays adjusted so that the zero- and first-order phase corrections along F_1 were 0° and 90°, respectively, to eliminate baseline curvature encountered otherwise (*38*).

The ^{13}C-^{1}H HSQC experiment at ^{13}C natural abundance was carried out with an aqueous sample of hPTH(1−31)-NH_2 with a peptide concentration of 1.2 mM. To improve the spectral quality, the H_2O solvent was replaced by D_2O after the buffered peptide solution was dried on a SpeedVac apparatus. A NOESY spectrum was acquired for the peptide sample in D_2O with a mixing time of 200 ms and at 278 K on the 800 MHz spectrometer, followed by a ^{13}C-^{1}H HSQC spectrum with spectral widths of 9980.04 Hz in the proton and 14084.08 Hz in the ^{13}C dimensions, respectively. Phase-sensitive detection was achieved using the States-TPPI scheme along the ^{13}C dimension with a total of 350 FIDs each of 1024 data points. The ^{1}H carrier was placed on the H_2O proton resonance, and the ^{13}C carrier was set to 37.5 ppm (in reference to DSS whose chemical shift was set to zero). Decoupling of the ^{13}C nuclei during acquisition of the proton FIDs was achieved using the GARP sequence (*39*) with a field strength of 3.1 kHz.

The NMR data were processed using nmrPipe (*40*) and/or using the XWIN-NMR software program running on Silicon Graphics computer workstations. The t_1 increments were extended by linear prediction to 512 and zero-filled to 1024 data points before the application of the window

functions. A squared-cosine window function was used for both time dimensions prior to Fourier transformation and polynomial baseline correction. Chemical shifts of all proton resonances and of the carbon resonances were referenced internally to that of DSS which was set to 0 ppm. The chemical shift of the water proton resonance was determined to be 4.98 ppm at 5 °C. Spectral analysis and resonance assignments were carried out on plotted spectra and on Silicon Graphics computer workstations with the software program PRONTO (*41*).

Assignments of Proton and Carbon-13 Resonances. Sequence-specific assignments of all proton resonances (Table S1) were achieved following standard procedures using a combination of TOCSY, COSY, and NOESY spectra. The TOCSY and COSY spectra were used to identify amino acid spin systems. NOESY (or ROESY) spectra were used to make sequential connections of the identified spin systems (Figure S1). The side-chain protons without scalar coupling were assigned on the basis of intraresidue NOESY connectivities. The ^{13}C resonances of the Cα carbons were assigned through the ^{13}C-^{1}H HSQC spectrum by use of the assigned CαH proton chemical shifts.

Collection of Conformational Constraints. Distance constraints were derived primarily from the NOESY spectra acquired at 800 MHz and at 5 °C with a peptide concentration of 1.2 mM. The use of the NOE data for the more concentrated peptide sample and at the low temperature of 5 °C was justified since practically the same NOE cross-peaks existed in NOESY (or ROESY) spectra of the concentrated sample at 25 °C and in a NOESY spectrum (NOE mixing time: 200 ms) for a sample with a reduced peptide concentration down to 0.2 mM (vida supra). NOESY data with mixing times of 100, 150, 200, and 250 ms for the high-concentration sample were used to assess and correct for the contributions of spin diffusion to the NOE intensities. The NOE peak volumes were integrated and calibrated based on the cross-peak intensities between proton pairs of known distances and were classified roughly as strong, medium, or weak, corresponding to distance upper bounds of 2.7, 3.5, and 5.0 Å, respectively. In addition, sequential and intraresidue NOEs were calibrated differently from medium- and long-range NOEs to allow for conformational flexibilities that may exist in the peptide backbone. An upper limit of 5.0 Å was set for all overlapped and partially overlapped NOE cross-peaks.

Measurement of the $^{3}J_{NH\alpha}$ coupling constants was carried out through fitting using the procedure of Titman and Keeler (*42*). Backbone dihedral restraints were derived from $^{3}J_{NH\alpha}$ coupling constants with the φ dihedral angles set to -60 ± 30 deg for $^{3}J_{NH\alpha} < 5.5$ Hz. The temperature coefficients of the backbone amide protons were obtained through fitting of the NH chemical shifts in a series of TOCSY spectra measured at experimental temperatures from 5 to 25 °C with 5 °C intervals. The slopes of the linear fittings were the coefficient constants and reported as ppb/K in Table 1.

Structure Calculations. Models of the three-dimensional structures were calculated by use of a protocol of distance geometry followed by simulated annealing, or DG/SA, implemented in the Xplor software program (*43*). Averaging for ambiguous proton distances was set to "SUM" for a proper treatment of unassigned prochiral protons and other NOE distances involving overlapped proton resonances (*44*−*48*). A set of 100 initial structures was generated by DG/SA using uniquely assigned NOE constraints. A total of 20 lowest energy structures were chosen to check for violations of the input NOE distances. The NOE constraints violated by >0.5 Å in more than 10 structures were checked for their original assignments and classification of distance ranges. Some ambiguous NOE cross-peaks were resolved on the basis of the consensus interproton distances in the 20 initial structures. These initial structures were refined using stimulated annealing calculations incorporating newly identified NOE distances. Neither hydrogen bonding nor electrostatic terms of the force field were used in any stage of the structure calculations. The van der Waals interactions were represented by a standard Lenard−Jones potential function with the weight gradually increased from 0.005 at the beginning to 4.0 at the end of the calculations. The NOE penalty function was a square-well potential with a force constant of 50 kcal mol^{-1} Å^{-2} . The maximum values of the force constants were set to 500 kcal mol^{-1} Å^{-2} for bond lengths and 500 kcal mol^{-1} rad^{-2} for both bond angles and impropers. The final stage of the structure calculations employed 499 uniquely assigned distance constraints, including 148 intraresidue, 175 sequential, and 149 medium- and 27 long-range distance upper and/or lower bounds along with 5 dihedral constraints (Table 3). Quality of the structure models was analyzed using PROCHECK-NMR (*49*). The structure models were visualized and manipulated by use of the Sybyl molecular graphics program (Tripos, Inc.).

NOE Simulations. Agreement of the computed structures with experimental NOE data was also verified through

Table 1: NH Proton Temperature Coefficients and $^{3}J_{NH\alpha}$ Coupling Constants[a] of hPTH(1−31)NH_2 in Aqueous Solution at pH 6.8

residue	Δδ (ppb/K)	$^{3}J_{NH\alpha}$ (Hz)
Ser1		
Val2		
Ser3	−7.7	
Glu4	−4.2	6.11
Ile5	−6.1	
Gln6	−4.7	
Leu7	−7.6	
Met8	−3.8	5.38
His9	−6.5	
Asn10	−6.9	
Leu11	−3.9	
Gly12	−1.8	
Lys13	−2.8	
His14	−8.2	
Leu15	−5.4	6.11
Asn16	−11.6	
Ser17	−8.5	
Met18	−1.52	5.87
Glu19	−7	4.65
Arg20	−9.48	
Val21	−0.94	5.13
Glu22	6.26	
Trp23	−8.34	4.4
Leu24	−9.56	5.38
Arg25	1.26	
Lys26	−4.26	
Lys27	0.36	
Leu28	−2.9	
Gln29	−0.84	
Asp30	−2.8	
Val31	−4.2	

[a] The coupling constants were measured at an experimental temperature of 298 K.

comparisons between experimental and calculated NOESY spectra. The NOE spectral simulations were performed using in-house programs, NOESIM, and GFIDSJ (*46*). The program NOESIM implements the ensemble-averaged relaxation matrix approach for interconverting conformations (*46*). The NOE intensities were calculated using an overall tumbling correlation time of 2.5 ns, estimated on the basis of the peptide molecular weight and the experimental temperatures (*50*) and using an internal correlation time of 25 ps for methyl rotations. The calculated NOE intensities were converted by GFIDSJ to simulated FIDs using experimentally determined proton chemical shifts (Table S1) along with standard coupling constants for each residue type (*51*) for a better representation of the simulated peak shapes. A uniform line width of 5 Hz was used for all protons and along both spectral dimensions. Simulated FID matrices were transformed into the frequency-domain NOESY spectra using identical processing parameters as with experimental data sets. NOESY simulations were performed with mixing times of 250, 200, 150, and 100 ms for comparison with their corresponding experimental NOESY data sets.

RESULTS

Backbone Folding of the hPTH(1−31)NH$_2$ Peptide in Solution. Figure 1, panel A shows the deviations of the chemical shifts from the corresponding random coil values for the CαH protons in hPTH(1−31)NH$_2$. Two stretches of residues with large and negative deviations are evident in the N- and C-terminal parts of the peptide sequence, suggesting that the PTH peptide under the studied conditions may consist of two distinct helical segments. The first helical region appears to encompass residue 3 to 13; the second helical segment may start from residue 17 and end at residue 31 at the C-terminus. In agreement with the CαH proton NMR results, the chemical shifts of the ^{13}Cα carbons also suggest two similar helical segments (Figure 1, panel B). The 17−31 segment displays large and positive deviations of the ^{13}Cα carbon chemical shifts from their random coil values. Positive deviations are also seen for residues 5−13, but somewhat less in magnitudes, suggesting that the N-terminal helix may be less populated conformationally than the longer C-terminal helix. Negative variations of the ^{13}Cα carbon chemical shifts were detected for residues 14−16, indicating that these residues in the middle of the peptide may assume extended or other than helical conformations. The $^3J_{NH\alpha}$ coupling constants also suggest that the conformation of hPTH(1−31)NH$_2$ is highly helical, especially for the C-terminal region, where residues have coupling constants of less than 6 Hz (Table 1). Taken together, both chemical shift deviations and measurable $^3J_{NH\alpha}$ coupling constants suggest preferences for helices in the N- and C-terminal regions of hPTH(1−31)NH$_2$ and the N-terminal helical segment may have somewhat more flexible conformations.

No slowly exchanging amide protons were found at 5 °C and at either pH 5.5 or 6.8 after the peptide was dissolved in D_2O (see Materials and Methods). However, the lack of slowly exchanging NH protons in hPTH(1−31)NH$_2$ at these high pH values is not surprising since the NH protons are protected only at acidic pH conditions even for the most well-folded helical structures (*29*, *52*, *53*). On the other hand, the amide protons of hPTH(1−31)NH$_2$ exhibit very small shifts with increasing temperature ($-\Delta\delta_{NH}/\Delta T$ < 5 ppb/K) for many residues and even positive shifts for some residues in the C-terminal region (Table 1). The observation of small negative and positive values for the NH temperature coefficients indicate that the amide protons of these residues must be involved in strong hydrogen-bonding interactions (*54*), such as those expected for a well-formed helical structure in the C-terminal region of hPTH(1−31)NH$_2$.

The two segments of secondary structures in hPTH(1−31)NH$_2$ are clearly defined by the many sequential NH/NH, CαH/NH (*i*, *i*+3), and CαH/Cβ*H* (*i*, *i*+3) NOEs (Figure 2), establishing a long helical structure encompassing residues 17−30 and a shorter helical segment spanning residues 4−10 at the N-terminal region. In addition, a large number of (*i*, *i*+3) and (*i*, *i*+4) NOEs involving the side-chain protons were observed, as to be discussed in later sections (vida infra). In the middle part of the peptide sequence, one CαH/NH(*i*, *i*+3) (*i* = 12) and two CαH/Cβ*H*(*i*, *i*+3) (*i* = 11 and 12) NOEs were found (Figure 2), indicating that the N-terminal helix may even extend to residue 14 or 15. The combination of the CαH proton and ^{13}Cα chemical shifts, the $^3J_{NH\alpha}$ coupling constants, NH proton temperature coefficients, and backbone NOEs therefore reveals that the hPTH(1−31)NH$_2$ peptide has well-formed, but perhaps relatively independent, helical structures localized in two distinct segments of the polypeptide backbone.

Capping Interactions and Side-Chain/Side-Chain NOEs in the hPTH(1−31)NH$_2$ Peptide. There are two potential N-capping and hydrophobic motifs (*55*, *56*) located at the beginning of both the N- and C-terminal helices of hPTH-(1−31)NH$_2$. The N-capping of the shorter helix is defined by the NOE contacts between Ser3 and Gln6 and by NOEs involving the side-chain protons of Val2 and Leu7 (Table 2). There are also possible NOE contacts between the methyl groups of Val2 and Leu7, but resonance overlaps prevented the observation of potential NOE cross-peaks among these protons. The N-capping and hydrophobic interactions for the C-terminal helix are defined by the many NOEs involving residues N16/E19 and L15/R20, respectively (Table 2). The positions of the two N-capping motifs can also be defined by the deviations of the ^{13}Cα chemical shifts (Figure 1, panel B), as the N-capping residue is expected to have an upfield-shifted ^{13}Cα resonance (*57*). Therefore, the C-terminal helix of hPTH(1−31)NH$_2$ starts at Ser17 with Asn16 serving as the capping residue. For the N-terminal helix, although the ^{13}Cα resonance of Glu4 could not be assigned unambiguously, the ^{13}Cα resonance of Ile5 displays a large downfield shift and that of Ser3 shows no variation from the random coil value (Figure 1, panel B). It is therefore reasonable to assume that the N-terminal helix starts at Glu4, and Ser3 is the N-cap residue in agreement with the existence of characteristic NOE patterns (vide supra). As compared to Asn16, the ^{13}Cα resonance of Ser3 is less shifted from the random coil value, which indicates that the N-terminal helix may be less populated than the C-terminal helix (*58*). This conclusion is further supported by the findings that most residues in the C-terminal helix have more shifted CαH proton and ^{13}Cα resonances than those in the N-terminal helix (Figure 1).

There are also many NOE connectivities among the side-chain protons of potential contact residues within a helical structure (Table 2). For example, in the N-terminal segment of the peptide, NOEs were observed between the side-chain

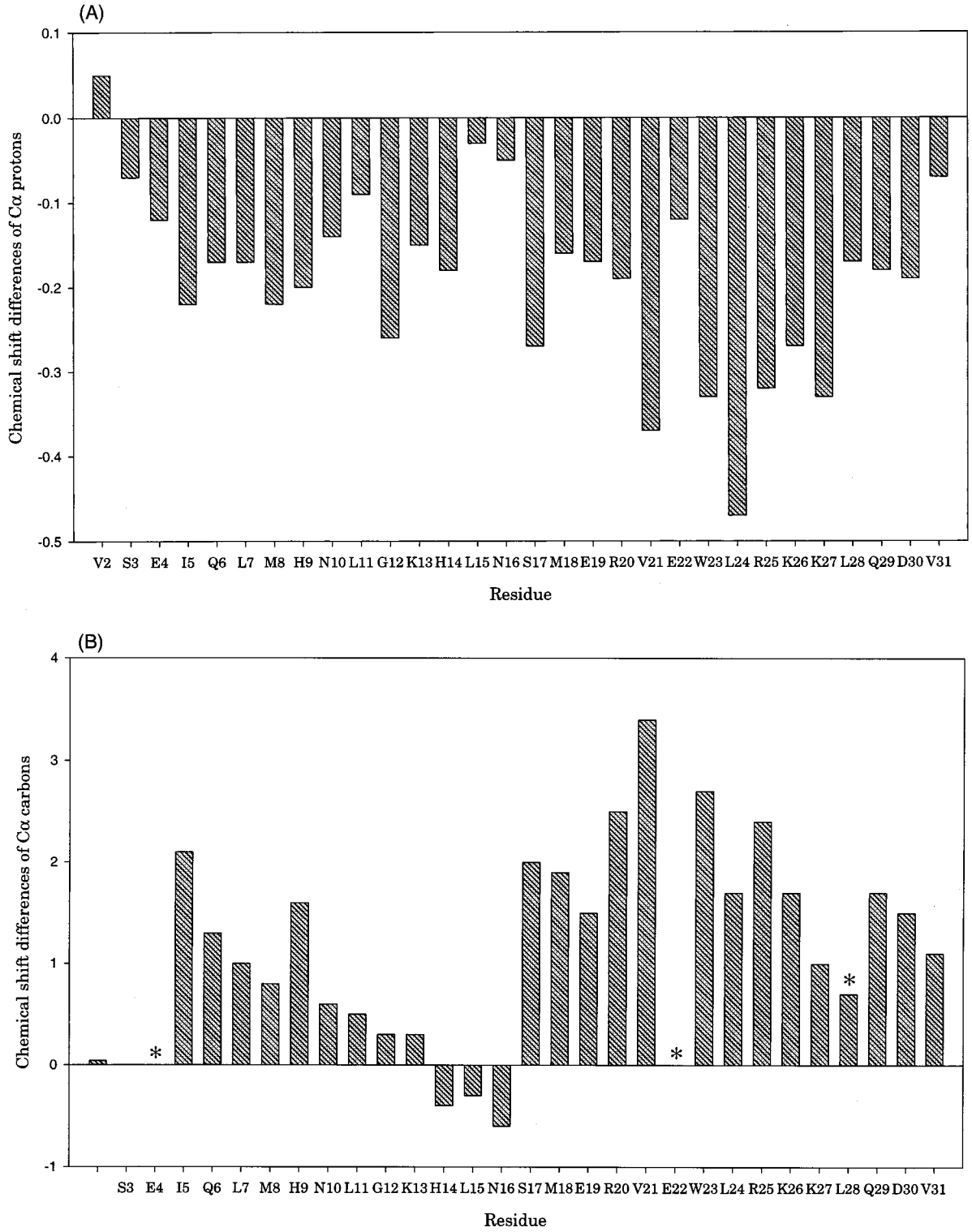

FIGURE 1: Deviations of the Cα proton and ^{13}C chemical shifts of hPTH(1−31)NH_2 from random-coil values. (A) Chemical shift deviations for the Cα proton resonances; (B) chemical shift deviations for the ^{13}Cα resonances. The asterisks in panel B indicate that the ^{13}Cα resonances for these residues could not be assigned unambiguously because of overlaps in their CαH proton resonances. The chemical shift values were obtained from the NMR spectra of hPTH(1−31)NH_2 in a buffered aqueous solution at pH 6.8 and at a temperature of 5 °C.

protons of Val2 and Asn10, Gln6 and Asn10, Leu7 and Asn10, and Gln6 and His9, and between Leu11 and His14. For the C-terminal helix, the NOEs involving side-chain protons were detected between residues 19 and 23, 21 and 25, 21 and 24, 22 and 26, 23 and 27, and 25 and 29. In addition, the aliphatic side-chain protons of Lys27 are all shifted upfield (lower chemical shift values) as compared to those of Lys13 and Lys26 (Table S1), in agreement with the NOE contacts between the side chains of Trp23 and Lys27. The NOEs between the Arg25 guanidino group and the Val21 methyl protons are especially noteworthy since the mobile and exchangeable nature of the guanidino amides usually prevent the observation of NOEs involving these protons (*59*). In addition, the side chain NϵH of Arg25 is shifted ~0.3 ppm downfield as compared to that of Arg20, another Arg residue in the hPTH(1−31)NH_2 peptide. Similar

Table 2: Summary of Representative NOEs Defining Capping and Side-Chain Packing Interactions in the Solution Structure of hPTH(1−31)NH_2

NOEs defining the N-cap and C-cap in the N-terminal helix	Ser3 NH − Gln6 CγHs; Ser3 NH − Gln6 NH; Ser3 CβHs − Gln6 NH; Ser3 CβHs − Gln6 CγHs; Leu7 NH − Val2 C$\gamma$$H_3$s; Leu7 C$\gamma$Hs − Val2 C$\gamma$$H_3$s; Gly12 C$\alpha$Hs − His9 C$\alpha$H
NOEs defining the N-cap in the C-terminal helix	Asn16 NH − Glu19 NH; Asn16 NH − Glu19 CβHs; Asn16 NH − Glu19 CγHs; Glu19 NH − Asn16 CβHs; Asn16 Nδ2Hs − Glu19 CβHs; Asn16 Nδ2Hs − Glu19 CγHs; Leu15 C$\delta$$H_3$s − Arg20 C$\delta$Hs; Leu15 C$\delta$$H_3$s − Arg20 NH; Leu15 C$\alpha$H − Arg20 C$\delta$Hs; Leu15 C$\delta$$H_3$s − Arg20 C$\alpha$H; Leu15 C$\delta$$H_3$s − Trp23 NH; Leu15 C$\delta$$H_3$s − Trp23 C$\epsilon$3H; Leu15 C$\delta$$H_3$s − Trp23 N$\epsilon$1H; Leu15 C$\delta$$H_3$s − Trp23 C$\zeta$3H
NOEs defining side-chain packing within the two helices	In the N-terminal helix: Val2 C$\gamma$$H_3$s − Gln6 C$\gamma$Hs; Val2 C$\gamma$$H_3$s − Gln6 N$\epsilon$2Hs; Val2 C$\gamma$$H_3$s − Asn10 N$\delta$Hs; Gln6 N$\epsilon$2Hs − His9 C$\delta$2H; Gln6 C$\beta$Hs − Asn10 N$\delta$2Hs; Gln6 C$\gamma$Hs − Asn10 N$\delta$2Hs; Leu7 C$\delta$$H_3$s − Asn10 N$\delta$2Hs; Leu11 C$\delta$$H_3$s − His14 C$\epsilon$1H In the C-terminal helix: Leu15 C$\delta$$H_3$s − Glu19 C$\gamma$Hs; Glu19 C$\beta$Hs − Trp23 C$\delta$1H; Val21 C$\gamma$$H_3$s − Arg25 N$\epsilon$H; Val21 C$\gamma$$H_3$s − Arg25 N$\eta$Hs; Val21 C$\gamma$$H_3$s − Arg25 C$\delta$Hs; Glu22 C$\gamma$Hs − Lys26 C$\epsilon$Hs; Glu22 C$\gamma$Hs − Lys26 C$\delta$Hs; Trp23 N$\epsilon$1H − Lys27 C$\epsilon$Hs; Trp23 N$\epsilon$1H − Lys27 C$\delta$Hs; Trp23 C$\epsilon$3H − Lys27 C$\delta$Hs; Trp23 C$\delta$1H − Lys27 C$\gamma$Hs; Arg25 C$\beta$Hs − Gln29 C$\gamma$Hs; Arg25 C$\beta$Hs − Gln29 N$\epsilon$2Hs
NOEs defining contacts between the two helices	Gly12 CαHs − Trp23 Cζ3H; Gly12 CαHs − Trp23 Cη2H; Gly12 CαHs − Trp23 Cδ1H; Gly12 CαHs − Trp23 Nϵ1H; Met8 CβHs − Trp23 Cζ2H; Met8 CβH − Trp23 Cη2H; Met8 CβH − Trp23 Cæ3H; Gly12 CαHs − Leu15 NH; Gly12 CαHs − Leu15 C$\delta$$H_3$s; Gly12 C$\alpha$Hs − Leu15 C$\gamma$H; Gly12 NH − Leu15 C$\delta$$H_3$s; Gly12 C$\alpha$Hs − Leu15 C$\beta$Hs

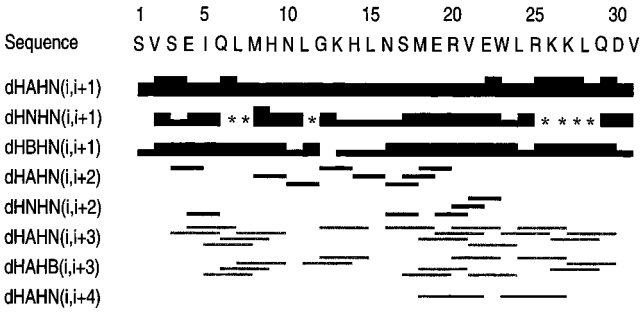

FIGURE 2: Summary of backbone NOEs observed for the hPTH-(1−31)NH_2 peptide. The experimental conditions: the peptide concentration, 1.2 mM; sample temperature, 5 °C; NOE mixing times, 100, 150, 200, and 250 ms.

NMR characteristics of Arg side-chain protons were observed for the conantokin-G and conantokin-T peptides, both of which have well-defined helical structures in solution (*29*, *30*).

In addition to expected NOEs pertaining to helical structures, there are also long-range NOEs from residues Met8 and Gly12 to the aromatic ring of Trp23, and between Gly12 and Leu15 (Table 2). The Leu15 residue therefore appears to serve as a bridge that may constrain the relative orientations of the two helices in hPTH(1−31)NH_2. The NOEs between Gly12 and the ring protons of Trp23 also exist in a series of NOESY spectra with a range of NOE mixing times of 100, 150, 200, and 250 ms. Corresponding, but weaker peaks were also observable in the NOESY (and ROESY) spectrum acquired at a higher temperature of 25 °C. Most importantly, those NOEs involving residues Met8, Gly12, Leu15, and Trp23 were consistently present in a NOESY spectrum of hPTH(1−31)NH_2 dissolved in D_2O (see Materials and Methods). In all, the intensities of these "interhelical" NOEs are still relatively weak as compared to other long-range NOEs, indicating that they may not represent very close contacts between the two helices or that there may be conformational averaging for the relative positioning of the two helical segments. Nevertheless, these interhelical NOE contacts suggest that there is a bend conformation in the middle of hPTH(1−31)NH_2 populated in high enough concentration to give rise to the observable and characteristic NOE interactions.

A Folded Solution Structure of the hPTH(1−31)NH_2 Peptide. The conformations of hPTH(1−31)NH_2 represented by the large number of observed NOEs was characterized in more detail through structure calculations using NOE-derived distances and some dihedral constraints derived from coupling constants. Structure calculations proceeded in a stage-wise fashion whereby the helical segments were first defined by use of the NOEs characterizing helical conformations (Figure 2) followed by the incorporation of side-chain and interhelical NOEs (Table 2) to define the tertiary contacts. The structure of the hinge region already took a bend shape even before the incorporation of all the interhelical contacts, e.g., in the absence of the very long range distance constraints between the side-chain protons of Met8 and Trp23. A set of 100 structures was then calculated using all 499 distance restraints derived from 148 intraresidue, 175 sequential, and 149 medium- and 27 long-range NOEs along with 5 dihedral angles. All calculations produced structures with a common fold that were in good agreement with the experimental NMR constraints. A total of 20 final structures with the lowest energy were chosen to represent the folded conformation of hPTH(1−31)NH_2 (Figure 3). All these structures satisfied all the input experimental constraints with minimal deviation from ideal covalent geometry (Table 3).

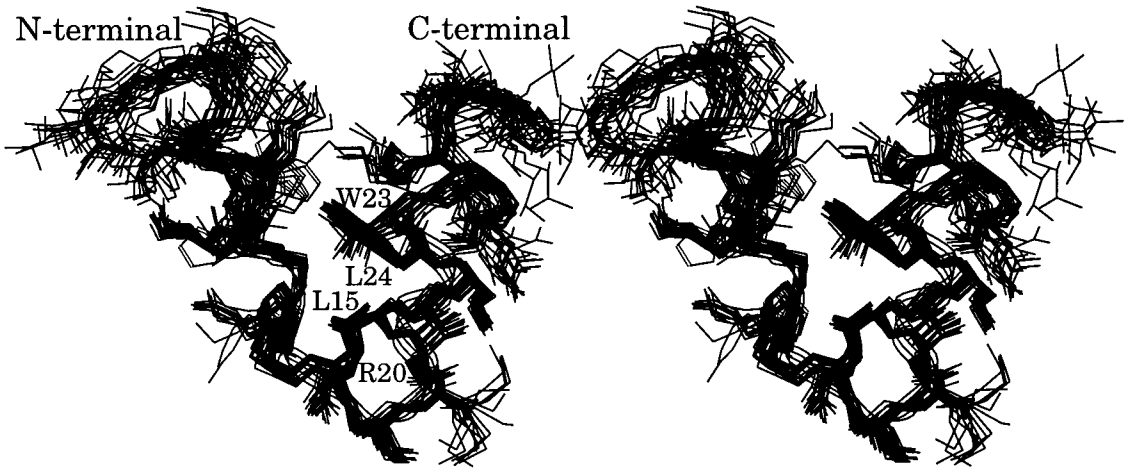

FIGURE 3: Cluster of 20 structures calculated by use of NOE distance constraints. All the structure models were superimposed using the backbone heavy atoms of residues 3−30. The residue labels illustrate well-defined side-chain positions for those residues in the C-terminal helical region. The line ribbon emphasizes a V-shaped conformation for hPTH(1−31)NH_2 with two helical segments, one for the N-terminal and the second for the C-terminal region, joined by hinge residues in the middle of the sequence. The atomic coordinates of the model structures have been deposited with the Protein Data Bank (PDB accession number 1FVY).

Table 3: Structural Statistics for the 20 Final Structures of hPTH(1−31)NH_2

distance constraints	
intraresidue ($i - j = 0$)	148
sequential ($\|i - j\| = 1$)	175
medium-range ($2 \leq \|i - j\| \leq 4$)	149
long-range ($\|i - j\| \geq 5$)	27
total	499
dihedral angle constraints	5
RMSD from the experimental constraints	
distance (Å)	0.062 ± 0.04
dihedral angle (°)	0.00 ± 0.0
RMSD from idealized covalent geometry	
bonds (Å)	0.0104 ± 0.0004
angles (°)	0.98 ± 0.08
impropers (°)	0.56 ± 0.09
mean energies (kcal/mol)	
E_{NOE}	92.7 ± 7.4
$E_{van\ der\ Waals}$	-493.3 ± 21.1
$E_{bond} + E_{angle} + E_{impropers}$	223.6 ± 11.4
atomic RMSD (Å)	
backbone (residues 3−30)	0.65 ± 0.08
heavy atoms (residues 3−30)	1.00 ± 0.11
Ramachandran plot	
% residues in the most favorable and additionally allowed regions	92.8
% residues in the generously allowed region	5.7
% residues in the disallowed region	1.4

Very importantly, none of the medium- and long-range NOE distances were violated by any of the selected structures, indicating that the set of NOE distance constraints, particularly those derived from the many side-chain/side-chain NOEs, are mutually consistent and can be accounted for by the minimal "ensemble" of calculated conformations (Figure 3). Superposition of the 20 structure models shows two stretches of well-defined helical conformations encompassing residues 3−11 and 16−30 at the N- and C-termini, respectively (Figure 3). Clearly, the overall structure is also relatively well-defined by the NMR data, with a mean rmsd of 0.65 ± 0.08 Å for backbone and 1.00 ± 0.07 Å for all heavy atoms of residues 3−30. The family of 20 structures also shows very good definitions of the backbone dihedral angles with an angular order parameter (*60*, *61*) greater than 0.88 for most residues.

The quality of the structure models was also verified through a calculation of predicted NOESY spectra on the basis of the three-dimensional structures shown in Figure 3. As compared with the experimental spectra, excellent agreement was found for medium- and long-range NOEs and for nonsequential CαH/NH NOEs in the fingerprint region and the NH/NH NOE connectivities. It is noteworthy that the long-range NOEs involving residues Met8, Gly12, and the ring protons of Trp23 and between Gly12 and Leu15 are all present in both the calculated and the experimental NOE spectra. The computed structures reveal close contacts between the methyl groups of Leu11 and the aromatic ring of Trp23, a structure feature brought about only by a bend conformation for residues Gly12, Lys13, His14, and Leu15. There were indeed experimental NOE contacts between the ring protons of Trp23 and the overlapped methyl protons of Leu7, Leu11, and/or Leu28 which were not utilized in structure calculations. Interestingly, none of the interhelical NOEs observed for hPTH(1−31)NH_2 were present in the calculated NOESY spectra (not shown) from the reported solution structure of hPTH(1−37) (*24*). It is therefore clear that the high quality of the folded structure (Figure 3) must be a result of the large number of experimental NOEs derived for the hPTH(1−31)NH_2 peptide, especially the many side-chain/side-chain NOE contacts for helical structures observable at increased field strength (800 MHz) and/or using the improved NMR pulse sequences (*29*, *30*).

Detailed comparisons of simulated and experimental NOESY spectra also identified the N-terminal helical structure as having much stronger experimental CαH/NH (*i*,*i*+1) NOEs than those in the C-terminal helix, indicating increased conformational flexibility in the N-terminal region. Indeed, the CαH/NH (*i*,*i*+1) NOEs all had stronger intensities than the CαH/NH (*i*,*i*+3) NOEs in the hPTH(1−31)-NH_2 peptide, as observed previously for the hPTH(1−37) peptides (*24*, *25*). More importantly, the intensity ratios of the CαH/NH (*i*,*i*+3) and the CαH/NH (*i*,*i*+1) NOEs were estimated to be 0.15−0.25 and 0.4−0.5 for the N- and the C-terminal helices, respectively, on the basis of the pair of well-resolved NOEs involving residues Ile5/Gln6 and Ile5/Met8 and the three pairs of NOEs involving residues Met18/

Glu19 and Met18/Val21, residues Val21/Glu22 and Val21/Leu24, and residues Leu24/Arg25 and Leu24/Lys27. The populations of the helical backbone conformations can be estimated from the ratios of the integrated intensities of the sequential $d_{\alpha N}$ and d_{NN} NOEs, as established previously (*62*, *63*). Using this method, the helical contents were determined to be ~40% (±15%) and ~75% (±15%), respectively, for the N- and the C-terminal helices, averaged over three pairs of residues Glu4/Glu5, Ile5/Gln6, and Met8/His9 and 6 pairs of residues Ser17/Met18, Met18/Glu19, Arg20/Val21, Val21/Glu22, Glu22/Trp23, and Leu24/Arg25. Similarly, the intensities of the interhelical NOE contacts reflect the population of the folded conformation (Figure 3) within the ensemble of solution conformations for hPTH(1−31)NH_2. Therefore, the intensities of the interhelical NOEs between residues Met8 and Trp23 and between Gly12 and Trp23 (Table 2) were compared with those of the characteristic helical (*i*,*i*+3) NOEs within the N- and C-terminal helical segments, producing intensity ratios of ~60% and ~30%, respectively, in relation to the two helices. Taken together, it appears that the structures computed for the hPTH(1−31)NH_2 peptide (Figure 3) may represent a significant population of the conformational ensemble and that this folded conformation is very likely formed cooperatively together with the individual helical segments.

The calculated structures contain two well-defined structural elements, i.e., capping boxes already identifiable on the basis of the NOE patterns, at the beginning of both the N- and C-terminal helices of hPTH(1−31)NH_2 (Figure 3). The amide protons of residues 3 and 16 are all directed toward the C-terminal ends of the helical structures, as expected for such capping motifs (*56*). This structural disposition for the backbone NH protons of Ser3 and Asn16 are probably the results of their potential hydrogen bonding interactions with the side-chain oxygen atoms of Gln6 and Glu19, respectively, even though these hydrogen bonds are not discernible in the structure models (Figure 4) calculated purely by use of NMR distance constraints (see Materials and Methods). The side chains of the two pairs of residues, Val2/Leu7 and Leu15/Arg20, are in close proximity (Figure 4), defining them as the hydrophobic contacts present in helical capping motifs (*55*, *56*, *64*, *65*). The end of the N-terminal helix is terminated at residue Leu11 followed by Gly12 and Lys13 frequently found at such positions at the end of a helical structure (*56*, *66*). Inspection of the structure models in Figure 3 showed that there is a hydrogen bond between the carbonyl oxygen of Met8 and the backbone NH proton of Gly12 and a bifurcated hydrogen bond between the backbone NH proton of Lys13 and the carbonyl oxygens of His9 and Asn10, in agreement with the very small NH temperature coefficients for residues Gly12 and Lys13 (Table 1). In addition to these capping interactions, there are also many side-chain/side-chain contacts within the C-terminal helix of hPTH(1−31)NH_2. On one side of this helix, there are side-chain pairs of Glu22−Arg25, Glu22−Lys26, and Arg25−Gln29 that can form potential ion-pair and/or hydrogen bonding interactions. It is very likely that the NϵH proton of Arg25 is involved in a hydrogen bond since this proton has a very downfield shifted proton resonance (by ~0.3 ppm). On the opposite face of the helix, there are characteristic hydrophobic interactions involving the large aromatic side chain of Trp23 packing against the aliphatic

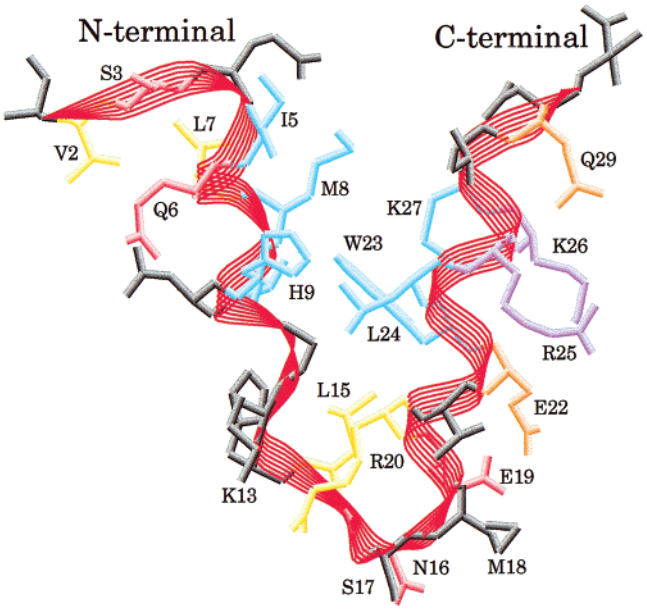

FIGURE 4: Representative structure of hPTH(1−31)NH_2 (from Figure 3) showing two helical segments (in red) along with capping and side-chain packing interactions. The N-capping residues are shown in red, and the associated hydrophobic contacts within the N-caps are shown in yellow. The positively charged residues Arg25 and Lys26 are colored in purple; residues Glu22 and Gln29 are in orange, indicating potential salt-bridge and/or hydrogen-bonding interactions with Arg25 and/or Lys26. Colored in blue are those residues, e.g., Ile5, Met8, His9, Trp23, Leu24, and Lys27, that may be involved in hydrophobic contacts, as discussed in the text. The side chains of residues Ser3, Gln6, Asn16, and Glu19 can form potential hydrogen bonds with specific backbone NH protons, that are, however, not defined by the NMR distance constraints (Figure 3).

side chains of Leu24 and Lys27. There are also long-range packing interactions between the side chains of Leu15 and Trp23, continuing to residues Leu24 and Leu28. As seen from Figures 3 and 4, the side chains of Ile5, Met8, and His9 are arranged into a cluster of nonpolar contacts within the helical structure for the N-terminal segment. There is also a linear array of hydrophobic residues from Val2, to Leu7, to Leu11 and continuing on to His14 and Leu15 in the hinge region. However, there are generally less complimentary charge/polar and hydrophobic packing interactions in the shorter N-terminal helix of hPTH(1−31)NH_2, which may explain its apparently higher conformational flexibility as compared to the well-structured nature of the C-terminal helix.

The folded structure of hPTH(1−31)NH_2 is likely an example of two helical secondary structures consolidated into a supersecondary structure solely by helical capping interactions, as proposed recently (*53*, *56*). There are six residues, Leu11, Gly12, Lys13, His14, Leu15, and Asn16, in the hinge region of the hPTH(1−31)NH_2 structure, that link the N-terminal helix to the C-terminal helix (Figure 4). Residue Leu11 occupies the C-cap position of the N-terminal helix and Asn16 at the N-cap position of the C-terminal helix. Residues Gly12, Lys13, and His14 appear to provide additional C-capping interactions, particularly in the form of a hydrogen bond from the backbone NH proton of Gly12 to the backbone carbonyl oxygen of residue Met8, as expected in an α_L motif for helix termination (*56*, *66*). However, there are no packing interactions between the side

chains of residue Met8 and His14, but the side chains of residues Leu11 and His14 appear to have close contacts (Figure 3), which are unexpected in standard helix termination motifs (*56*, *66*). In addition, residues Leu11, His14, Leu15, and Trp23 are arranged in a compact cluster of hydrophobic residues, linking the two helices into a roughly V-shaped supersecondary structure for hPTH(1−31)NH_2.

DISCUSSION

Origin of the Conformational Stability of the hPTH(1−31)NH_2 Peptide. The hPTH(1−31)NH_2 molecule contains a similar helical content as compared to hPTH(1−34) determined on the basis of circular dichroism (CD) measurements (*7*). Indeed, the same type of secondary structures are present in hPTH(1−31)NH_2, namely, a short N-terminal helix followed by a loop and then by a long C-terminal helix (Figure 4), as in hPTH(1−34) (*26*) and in hPTH(1−37) (*24*). The CD-determined helical populations were ∼26% for both hPTH(1−31)NH_2 and hPTH(1−34)NH_2 (*7*, *16*). The average helical content for hPTH(1−31)NH_2 is ∼40% (±10%) by use of NOE intensity ratios measured at a lowered temperature of 5 °C instead of ambient temperatures (*7*, *16*). Considering the limits of detection for both CD and NMR, these results indicate that there are no conformational destabilization or little structural alterations in the hPTH-(1−31)NH_2 fragment as compared to hPTH(1−34) or hPTH-(1−37). A helix−turn−helix or a U-shaped conformation has also been inferred for the hPTH(1−37) peptide in a salted aqueous solution at pH 6 (*24*), on the basis of nuclear Overhauser effects defining a turn conformation for residues His14 to Ser17 (Figure 5). However, the presence of this "folded" or U-shaped conformation was disputed in a study of the solution conformations of hPTH(1−34) under a variety of solution conditions (*26*). The latter study questioned the existence of the U-shaped structure as the only conformer for hPTH(1−34) but did not exclude the possibility of the U-shaped conformation as one component of the conformational ensemble in solution. Our results here indicate that the U-shaped conformation represents a significant population of the conformational ensemble and is preferred for at least the folded conformations of the hPTH(1−31)NH_2 peptide. Indeed, the latest NMR study again indicates the presence of a folded or U-shaped conformation for the hPTH-(1−34) peptide under near physiological conditions (*67*).

One of the hallmarks in the studies of human PTH fragments, namely, hPTH(1−34) and hPTH(1−37), has been the finding of a helical conformation for the C-terminal region (Figure 5), which is stable under a variety of solution conditions (*24*−*26*). In fact, the 13−34 and 16−34 subfragments of human PTH were found to retain most of the helix signature in the CD spectra (*7*, *16*), while the helical conformation is mostly lost in the hPTH(20−34) peptide. These observations clearly indicate that the C-terminal helix of hPTH(1−34) along with the capping residues Leu15−Arg20 must be an autonomously stable structural subdomain. The solution structure of hPTH(1−37) showed that the C-terminal helix is stabilized by a defined turn preceding the helix (Figure 5) with characteristic capping interactions involving either Asn16 or Ser17 as the N-cap residue (*24*). The folded structure derived for hPTH(1−31)NH_2 shows clearly that the N-cap residue is Asn16 along with reciprocal side-chain/backbone hydrogen bonds involving residue Glu19

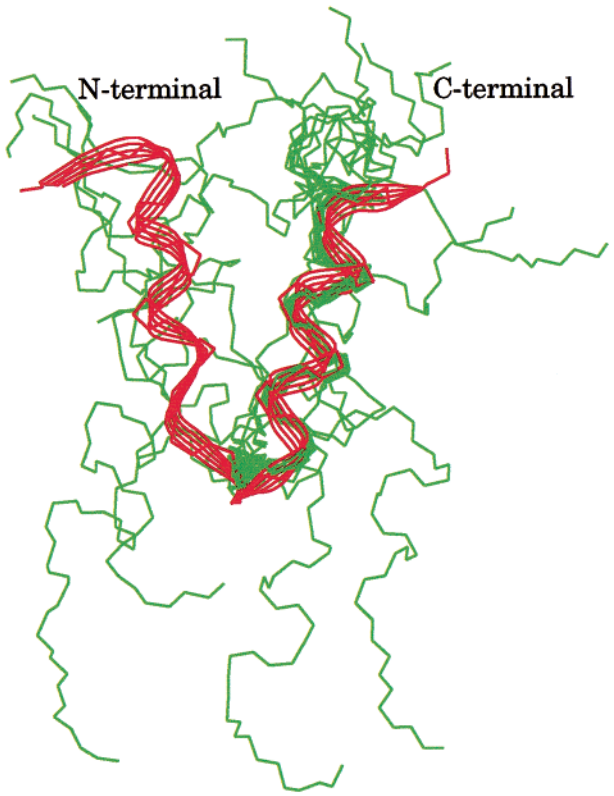

FIGURE 5: Comparison of the well-folded conformation of hPTH-(1−31)NH_2 with that of hPTH (1−37). The two sets of structures are overlaid through superposition of the backbone heavy atoms of residues Asn16 to Gln29. A total of 12 different conformations were used for hPTH (1−37), that were derived from NMR distance constraints (*24*). Only one conformer was used for hPTH(1−31)-NH_2, which is shown here as a backbone ribbon (in red).

as well as hydrophobic contacts among residues Leu15, Arg20, and Trp23 (Figures 3 and 4). In fact, hPTH(1−37) was one of the first few peptides that were found to contain well-defined N-cap and hydrophobic interactions stabilizing a helical structure (*24*, *55*, *64*). In the structure of hPTH-(1−31)NH_2, there are also extensive side-chain packing interactions involving residues Glu22−Arg25, Glu22−Lys26, Arg25−Gln29, Leu15−Trp23, Trp23−Leu24, Trp23−Lys27, and Leu24−Leu28 (Figures 3 and 4). It is therefore quite clear that the conformational stability of the C-terminal helix of the PTH peptides must be determined largely by the N-cap and side-chain packing interactions that favor the formation of the helix structure in both peptides and proteins (*56*, *65*).

The amino acid sequence of hPTH(1−34) or hPTH(1−37) contains another potential N-cap and hydrophobic motif, namely, of Val2−Ser3−Glu4−Ile5−Gln6−Leu7 at the start of the apparently more flexible N-terminal helix. The Val2/Leu7 alkyl side chains are involved in hydrophobic interactions, and the Ser3/Gln6 residue pair is engaged in hydrogen bonding in the structure of hPTH(1−31)NH_2 (Figures 3 and 4). It has been shown that the removal of Ser1 had no effect on the conformational properties of hPTH(2−37), while truncation of the two N-terminal residues Ser1 and Val2 as in hPTH(3−37) or three N-terminal residues Ser1, Val2, and Ser3 in hPTH(4−37) almost completely abolishes the N-terminal helical conformation but is without significant effects on the C-terminal helical structure (*25*). These

observations indicate that both the capping interactions between residues Ser3 and Gln6 and the hydrophobic interactions between Val2 and Leu7 are important determinants for the conformational stability of the N-terminal helix of hPTH(1−37), as predicted by the structure of hPTH(1−31)NH_2 (Figures 3 and 4). The existence and proposed importance of N-capping interactions in the N-terminal helix is also supported by the identification of a similar N-cap motif in bovine PTH(1−37) stabilized by hydrophobic residues Val2 and Phe7 (substituting for Leu7 in human PTH) (*67*). The conformational properties of the N-terminally truncated fragments of hPTH(1−37) (*25*) also suggest that the two helical segments in hPTH(1−37) may have intimate contacts only between the end of the N-terminal helix and the beginning of the C-terminal helix as in a possibly V-shaped conformation (Figure 4) also for hPTH(1−37). Interestingly, it was found that the hPTH(1−19) peptide has little or no helical contents in aqueous solution in contrast to the C-terminal peptide hPTH(13−34) (*16*). Therefore, the N-terminal helix of hPTH(1−31)NH_2, hPTH(1−34), or hPTH(1−37) must require the presence of a well-structured C-terminal helix to maintain a proper conformational stability in solution.

The apparent stability of the hPTH(1−31)NH_2 structure is possibly a result of the removal of residues His32, Asn33, and Phe34 or His32, Asn33, Phe34, Val35, Ala36, and Leu37 which are unstructured in hPTH(1−34) and hPTH(1−37), respectively (*24*−*26*). Residue preferences for helix termination signals predict that the C-terminal helix in hPTH(1−31), hPTH(1−34), or hPTH(1−37) may only extend as far as Leu28 or Gln29, in agreement with experimental findings reported here for hPTH(1-31)NH_2 and with the other PTH peptides (*20*, *22*, *24*−*26*). Core helical conformations are little affected by C-terminal extensions of the PTH peptides beyond residue 37, as demonstrated recently for hPTH(1−39) (*67*). In the structure of hPTH(1−31)NH_2, residues Asp30 and Val31 appear to provide capping interactions to the C-terminal helix in the form of hydrogen bonds from their NH protons to the carbonyl oxygens of residues Lys26 and Lys27 (Figure 3), in agreement with a significant decrease of the helical content of hPTH(1−29)NH_2 after removing residues Asp30 and Val31 from hPTH(1−31)NH_2 (*7*). Inclusion of residues His32, Asn33, and Phe34 in hPTH(1−34) or the additional Val35, Ala36, and Leu37 in hPTH(1−37) may therefore destabilize the C-terminal helix found in hPTH(1−31)NH_2 since these additional residues may distract capping interactions in favor of nonspecific hydrophobic contacts. The hPTH(1−34) peptide under identical solution conditions as utilized here had somewhat broader proton resonances and a narrower dispersion of its NH proton resonances as compared to hPTH(1−31)NH_2 (unpublished observations), indicating a reduced conformational stability for the longer peptide. Interestingly, the same characteristic NOEs involving Met8, Gly12, Leu15, and Trp23 are also present in the hPTH(1−34) peptide (spectra not shown), suggesting the existence of the V-shaped conformation even for hPTH(1−34). Indeed, the hPTH(1−34) peptide was recently found to assume a similarly folded (or U-shaped) conformation as hPTH(1−37) and bPTH(1−37) (*67*). The existence of a folded structure for hPTH(1−31)NH_2 and for other PTH peptides therefore again highlights the importance of hydrophobic residues at strategic sequence locations for the conformational stability of bioactive peptides and protein fragments (*29*, *55*, *56*, *63*−*66*, *68*).

Implications of the hPTH(1−31)NH_2 Structure for its Biological Activities. It has been well-established that the affinity for the PTH−receptor interactions is determined principally by residues 14−34 or the C-terminal helical structure of hPTH(1−34) (*69*, *70*). On the other hand, residues at the end and beyond the well-structured C-terminal helix are responsible for some of the biological activities of hPTH(1−34), since a peptide with as few as residues 29−32 was found to activate PKC in rat osteosarcoma (ROS) cells (*8*−*11*). It has also been found that intact N-terminal residues are absolutely required for the adenylyl cyclase (AC) stimulating activity of hPTH(1−34) and consequently the regulation of calcium levels in the blood by hPTH(1−37) (*8*, *25*). In addition, AC activation was found to require at least the first 28 residues of hPTH or hPTH(1−28)NH_2 (*6*, *7*). Therefore, the conformational stability of the N-terminal helix is likely very important for the osteogenic/anabolic activities of PTH peptides. Interestingly, the shorter (1−31)-NH_2 fragment of hPTH was found to have differentially enhanced AC-stimulating activities of PTH required for the promotion of bone growth (*9*, *12*, *13*) as opposed to stimulation of phospholipase Cβ. Our studies here revealed that the same linear hPTH(1−31)NH_2 peptide has the best defined solution structure (Figure 3) among all bioactive PTH fragments. It has been shown recently that the anabolic activites of hPTH(1−31)NH_2 can be further enhanced by replacing Lys27 with Leu and by cyclization of the side chains of Glu22 and Lys26 through lactam formation (*2*, *31*). The folded structure of hPTH(1−31)NH_2 indeed places the side chains of residues Glu22 and Lys26 in spatial proximity (Figures 3 and 4). In addition, substitution of Lys27 by Leu would enhance the interactions between the side chains of residues Trp23 and Lys27 through increased hydrophobic contacts between Trp23 and Leu27. Both of these modifications are therefore expected to increase the population and the conformational stability of the C-terminal helical structure in hPTH(1−31)NH_2, in exact agreement with experimental observations (*31*).

In a most recent investigation, significant enhancement of the AC-stimulating activity was observed when residues Ser1, Met8, Met18, Glu22, and Lys27 of hPTH(1−31)NH_2 were replaced by Ala1, Nle8, Lys18, Asp22, and Leu27, respectively (*71*). Positive impact of these multiple substitutions on biological activities can be rationalized by the V-shaped structure of hPTH(1−31)NH_2 (Figure 3), as discussed in part in the previous sections. The Met18 to Lys18 substitution in particular may stabilize the C-terminal helix of hPTH(1−31)NH_2 as Lys18 would expand the electrostatic and/or salt-bridge/hydrogen-bonding network (Figure 4) involving residues Lys18, Asp22, Arg25, Lys26, and Gln29 in the analogue peptide. Residues Lys18 and Asp22 of the substituted peptide can accommodate a lactam bridge between their side chains (*71*), as one would expect from the folded structure of hPTH(1−31)NH_2 (Figures 3 and 4). Residues Lys26 and Asp30 can also tolerate somewhat the cyclization of their side chains (*31*, *71*) even though Asp30 is outside the well-structured helical region, serving as a C-cap residue (Figure 3). The AC-stimulating activity of the analogue peptide is further enhanced by the formation of two lactam bridges between the side chains of residues

Lys18 and Asp22 and of residues Lys26 and Asp30, respectively (*71*). Taken together, these results show clearly that stabilization of the C-terminal helix in hPTH(1−31)-NH_2 generally leads to enhanced AC-stimulating activity and consequently increased anabolic/osteogenic activities of PTH peptides.

Very interestingly, little change of AC activities was observed by the introduction of a third lactam bridge between residues Lys13 and Asp17 (for the native residue Ser17) into the Lys18−Asp22 and Lys26−Asp30 doubly constrained peptide (*71*). In addition, the Lys13−Asp17 cyclization was found to have little effect on the activities of the analogue hPTH(1−31)NH_2 peptide constrained by either the Lys18−Asp22 or the Lys26−Asp30 lactam bridge (*71*). Residues Lys13 and Ser17 are indeed placed into spatial proximity by the V-shaped conformation of hPTH(1−31)NH_2 (Figures 3 and 4). However, side-chain cyclization between these two residues may reduce the conformational stability of the C-terminal helix as it may displace the side chain of Arg20 from having critical interactions with the side chain of Leu15, observed here in hPTH(1−31)NH_2 (Figure 3) and previously in hTPH(1−37) (*24*). On the basis of the activity profiles and conformational behaviors of various substituted and constrained analogues of hPTH(1−31)NH_2, it was concluded that the human parathyroid hormone must bind to its receptor in an extended or a straight helical conformation *(71)*, as opposed to a U-shaped or rather the V-shaped conformation (Figures 3−5) or to a flexibly linked double helix conformation described previously (*26*, *72*). However, a single side-chain/side-chain bridge cannot guarantee the formation of helical structures for all the five residues in the hinge region, namely, residues Gly12, Lys13, His14, Leu15, and Asn16. Therefore, it will be extremely important to determine the biological activities of a PTH peptide constrained into the "folded" and V-shape conformation to assess whether the solution structure determined here for hPTH(1−31)NH_2 (Figure 3) represents at least one of the bioactive conformations for PTH peptides. This is especially true if one considers the fact that the parathyroid hormone has pleiotropic activities (*1*−*3*), which may be expressed through the binding to different receptor subtypes of which two have been identified to date (*72*). Better understanding of the structure−activity relationship of the PTH molecules will also come from the characterization of the solution conformations of selectively cyclized PTH analogues and ultimately the three-dimensional structures of PTH peptides in complex with well-defined receptor targets.

CONCLUSIONS

The solution structure of hPTH(1−31)NH_2 contains predominantly a short N-terminal helical segment for residues 3−11, including the helix capping residues 3 and 11, and a long C-terminal helix for residues 16−30. The two helical structures are reinforced by well-defined capping motifs and associated interactions at both ends of these helices. The long C-terminal helix has in addition many characteristic and complimentary charge/polar and hydrophobic side-chain packing contacts that contribute to the stability of helical structures. Unique capping and hydrophobic interactions at the end of the N-terminal and at the beginning of the C-terminal helix appear to consolidate the two helical structure elements into a roughly V-shaped overall conformation for at least the folded population of the hPTH(1−31)NH_2 peptide. Capping and side-chain packing interactions therefore may also play a major role in the conformational stability of hPTH(1−31)NH_2 and potentially other bioactive PTH fragments. Existence of well-folded conformations in this linear 1−31 peptide fragment and possibly other analogues of human PTH may be an important determinant for the biological activities of the PTH peptides in general and specifically for the osteogenic/anabolic activities of bone-building PTH analogues.

ACKNOWLEDGMENT

We are grateful to Surajit Bhattacharjya, Dmitri Tolkatchev, and Wim Vranken for their critical readings of the manuscript and helpful comments. Thanks are also due to Betty Zhu for help with structure calculations and molecular graphics.

SUPPORTING INFORMATION AVAILABLE

Proton resonance assignment of the hPTP(1−31)NH_2 peptide in aqueous solution at pH 6.8 and at 5 °C (Table S1). Fingerprint (NH-CαH) region of a NOESY spectrum of hPTH(1−31)NH_2 in aqueous solution at pH 6.8 and at 5 °C (Figure S1). This material is available free of charge via the Internet at http://pubs.acs.org.

REFERENCES

1. Broadus, A. E., and Stewart, A. F. (1994) in *The Parathyroids: Basic and Clinical Concepts* pp 259−294, Raven Press, New York.
2. Morley, P., Whitfield, J. F., and Willick, G. E. (1999) *Curr. Med. Chem. 6*, 1095−1106.
3. Potts, J. T., Jr., Gardella, T. J., Juppner, H., and Kronenberg, H. M. (1997) *J. Endocrinol. 154* Suppl, S15−21.
4. Potts, J. T., Jr, Tregear, G. W., Keutmann, H. T., Niall, H. D., Sauer, R., Deftos, L. J., Dawson, B. F., Hogan, M. L., and Aurbach, G. D. (1971) *Proc. Natl. Acad. Sci. U.S.A. 68-(1)*, 63−67.
5. Herrmann-Erlee, M. P., Heersche, J. N., Hekkelman, J. W., Gaillard, P. J., Tregear, G. W., Parsons, J. A., and Potts, J. T., Jr. (1976) *Endocr. Res. Commun. 3(1)*, 21−35.
6. Tregear, G. W., Van Rietschoten, J., Greene, E., Keutmann, H. T., Niall, H. D., Reit, B., Parsons, J. A., and Potts, J. T., Jr. (1973) *Endocrinology 93(6)*, 1349−1353.
7. Neugebauer, W., Barbier, J. R., Sung, W. L., Whitfield, J. F., and Willick, G. E. (1995) *Biochemistry 34(27)*, 8835−8842.
8. Chakravarthy, B. R., Durkin, J. P., Rixon, R. H., and Whitfield, J. F. (1990) *Biochem. Biophys. Res. Commun. 171(3)*, 1105−1110.
9. Jouishomme, H., Whitfield, J. F., Chakravarthy, B., Durkin, J. P., Gagnon, L., Isaacs, R. J., MacLean, S., Neugebauer, W., Willick, G., and Rixon, R. H. (1992) *Endocrinology 130(1)*, 53−60.
10. Jouishomme, H., Whitfield, J. F., Gagnon, L., Maclean, S., Isaacs, R., Chakravarthy, B., Durkin, J., Neugebauer, W., Willick, G., and Rixon, R. H. (1994) *J. Bone Miner. Res. 9(8)*, 1179−1189.
11. Azarani, A., Goltzman, D., and Orlowski, J. (1996) *J. Biol. Chem. 271(25)*, 14931−14936.
12. Rixon, R. H., Whitfield, J. F., Gagnon, L., Isaacs, R. J., Maclean, S., Chakravarthy, B., Durkin, J. P., Neugebauer, W., Ross, V., Sung, W., et al. (1994) *J. Bone Miner. Res. 9(6)*, 943−949.
13. Whitfield, J. F., Morley, P., Willick, G. E., Ross, V., Barbier, J. R., Isaacs, R. J., and Ohannessian-Barry, L. (1996) *Calcif. Tissue Int. 58(2)*, 81−87.

14. Fraher, L. J., Avram, R., Watson, P. H., Hendy, G. N., Henderson, J. E., Chong, K. L., Goltzman, D., Morley, P., Willick, G. E., Whitfield, J. F., and Hodsman, A. B. (1999) *J. Clin. Endocrinol. Metab. 84*, 2739−2743.
15. Whitfield, J. F., and Morley, P. (1995) *Trends. Pharmacol. Sci. 16(11)*, 382−386.
16. Neugebauer, W., Surewicz, W. K., Gordon, H. L., Somorjai, R. L., Sung, W., and Willick, G. E. (1992) *Biochemistry 31-(7)*, 2056−2063.
17. Coddington, J. M., and Barling, P. M. (1989) *Mol. Endocrinol. 3(4)*, 749−753.
18. Gronwald, W., Schomburg, D., Harder, M. P., Mayer, H., Paulsen, J., Wingender, E., and Wray, V. (1996) *Biol. Chem. Hoppe-Seyler 377(3)*, 175−186.
19. Barden, J. A., and Cuthbertson, R. M. (1993) *Eur. J. Biochem. 215(2)*, 315−321.
20. Wray, V., Federau, T., Gronwald, W., Mayer, H., Schomburg, D., Tegge, W., and Wingender, E. (1994) *Biochemistry 33-(7)*, 1684−1693.
21. Barden, J. A., and Kemp, B. E. (1993) *Biochemistry 32(28)*, 7126−7132.
22. Strickland, L. A., Bozzato, R. P., and Kronis, K. A. (1993) *Biochemistry 32(23)*, 6050−6057.
23. Kanaori, K., Takai, M., and Nosaka, A. Y. (1997) *Eur. J. Biochem. 249*, 878−885.
24. Marx, U. C., Austermann, S., Bayer, P., Adermann, K., Ejchart, A., Sticht, H., Walter, S., Schmid, F. X., Jaenicke, R., Forssmann, W. G., et al. (1995) *J. Biol. Chem. 270*, 15194−15202
25. Marx, U. C., Adermann, K., Bayer, P., Meyer, M., Forssmann, W. G., and Rosch, P. (1998) *J. Biol. Chem. 273*, 4308−4316.
26. Pellegrini, M., Royo, M., Rosenblatt, M., Chorev, M., and Mierke, D. F. (1998) *J. Biol. Chem. 273*, 10420−10427.
27. Fulton, D. B., Hrabal, R., and Ni, F. (1996) *J. Biomol. NMR 8*, 213−218.
28. Fulton, D. B., and Ni, F. (1997) *J. Magn. Reson. 129*, 93−97.
29. Warder, S. E., Chen, Z., Zhu, Y., Prorok, M., Castellino, F. J., and Ni, F. (1997) *FEBS Lett. 411*, 19−26.
30. Chen, Z., Blandl, T., Prorok, M., Warder, S. E., Li, L., Zhu, Y., Pedersen, L. G., Ni, F., and Castellino, F. J. (1997) *J. Biol. Chem. 273*, 16248−16258.
31. Barbier, J. R., Neugebauer, W., Morley, P., Ross, V., Soska, M., Whitfield, J. F., and Willick, G. E. (1997) *J. Med. Chem. 40*, 1373−1380.
32. Marion, D., and Wuthrich, K. (1983) *Biochem. Biophys. Res. Commun. 113*, 967−974.
33. Lippens, G., Dhalluin, C., and Wieruszeski, J.-M. (1995) *J. Biomol. NMR 5*, 327−331.
34. Griesinger, C., and Ernst, R. R. (1987) *J. Magn. Reson. 75*, 261−271.
35. Kadkhodaei, M., Hwang, T.-L., Tang, J., and Shaka, A. J. (1993) *J. Magn. Reson. A105*, 104−107.
36. Piotto, M., Saudek, V., and Sklenar, V. (1992) *J. Biomol. NMR 2*, 661−665.
37. Sklenar, V., Piotto, M., Leppik, R., and Saudek, V. (1993) *J. Magn. Reson. A102*, 241−245.
38. Ni, F. (1992) *J. Magn. Reson.* 99, 391−397.
39. Shaka, A. J., Barker, P. B., and Freeman, R. (1985) *J. Magn. Reson. 64*, 547−552.
40. Delaglio, F., Grzesiek, S., Vuister, G. W., Zhu, G., Pfeifer, J., and Bax, A. (1995) *J. Biomol. NMR 6*, 277−293.
41. Kjaer, M., Andersen, K. V., and Poulsen, F. M. (1994) *Methods Enzymol. 239*, 288−307.
42. Titman, J. J., and Keeler, J. (1990) *J. Magn. Reson. 80*, 640−646.
43. Brunger A. T. (1996) X-PLOR manual, version 3.843, Yale University.
44. Ni, F., Meinwald, Y. C., Vasquez, M., and Scheraga, H. A. (1989) *Biochemistry 28*, 3094−3105.
45. Ni, F., Zhu, Y., and Scheraga, H. A. (1995). *J. Mol. Biol. 252*, 656−671.
46. Ni, F. (1994) *Prog. NMR Spectrosc. 26*, 517−606.
47. Nilges, M. (1995) *J. Mol. Biol. 245*, 645−660.
48. Fletcher, J. I., Smith, R., O'Donoghue, S. I., Nilges, M., Connor, M., Howden, M. E., Christie, M. J., and King, G. F. (1997) *Nat. Struct. Biol. 4*, 559−566.
49. Laskowski, R. A., Rullmannn, J. A., MacArthur, M. W., Kaptein, R., and Thornton, J. M. (1996) *J. Biomol. NMR 8*, 477−486.
50. Cantor, C. R., and Schimmel, P. R. (1980) in *Biophysical Chemistry*, p 461, W. H. Freeman and Company, San Francisco.
51. Bundi, A., and Wuthrich, K. (1979) *Biopolymers 18*, 285−297.
52. Padmanabhan, S., and Baldwin, R. L. (1994) *J. Mol. Biol. 241*, 706−713.
53. Sukumar, M., and Gierasch, L. M. (1997) *Fold Des. 2*, 211−222.
54. Baxter, N. J., and Williamson, M. P. (1997) *J. Biomol. NMR 9*, 359−369.
55. Munoz, V., Blanco, F. J., and Serrano, L. (1995) *Nat. Struct. Biol. 2*, 380−385.
56. Aurora, R., and Rose, G. D. (1998) *Protein Sci. 7*, 21−38.
57. Gronenborn, A. M., and Clore, G. M. (1994) *J. Biomol. NMR 4*, 455−458.
58. Guerois, R., Cordier-Ochsenbein, F., Baleux, F., Huynh-Dinh, T., Neumann, J. M., and Sanson, A. (1998) *Protein Sci. 7*, 1506−1515.
59. Yamazaki, T., Pascal, S. M., Singer, A. U., Formann-Kay, J. D., and Kay, L. E. (1995) *J. Am. Chem. Soc. 117*, 3556−3564.
60. Pallaghy, P. K., Duggan, B. M., Pennington, M. W., and Norton, R. S. (1993) *J. Mol. Biol. 234*, 405−420.
61. Hyberts, S. G., Goldberg, M. S., Havel, T. F., and Wagner, G. (1992) *Protein Sci. 1*, 736−751.
62. Bradley, E. K., Thomason, J. F., Cohen, F. E., Kosen, P. A., and Kuntz, I. D. (1990) *J. Mol. Biol. 215*, 607−622.
63. Ni, F., Ripoll, D. R., and Purisima, E. O. (1992) *Biochemistry 31*, 2545−2554.
64. Ni, F., Carpenter, K. A., Ripoll, D. R., Sanderson, S. D., and Hugli, T. E. (1996) *Biopolymers 38*, 31−41.
65. Seale, J. W., Srinivasan, R., and Rose, G. D. (1994) *Protein Sci. 3*, 1741−1745.
66. Aurora, R., Srinivasan, R., and Rose, G. D. (1994) *Science 264*, 1126−1130.
67. Marx, U. C., Adermann, K., Bayer, P., Meyer, M., Forssmann, W. G., and Rosch, P. (2000) *Biochem. Biophys. Res. Commun. 267*, 213−220.
68. Dyson, H. J., and Wright, P. E. (1996) *Annu. Rev. Phys. Chem. 47*, 369−395.
69. Caulfield, M. P., McKee, R. L., Goldman, M. E., Duong, L. T., Fisher, J. E., Gay, C. T., DeHaven, P. A., Levy, J. J., Roubini, E., Nutt, R. F., et al. (1990) *Endocrinology 127*, 83−87.
70. Gardella, T. J., Wilson, A. K., Keutmann, H. T., Oberstein, R., Potts, J. T., Jr., Kronenberg, M., and Nussbaum, S. R. (1993) *Endocrinology 132*, 2024−2030.
71. Condon, S. M., Morize, I., Darnbrough, S., Burns, C. J., Miller, B. E., Uhl, J., Burke, K., Jariwala, N., Locke, K., Krolikowski, P. H., Vasant Kumar, N., and Labaudiniere, R. F. (2000) *J. Am. Chem. Soc. 122*, 3007−3014.
72. Rolz, C., Pellegrini, M., and Mierke, D. F. (1999) *Biochemistry 38*, 6397−6405.

BI000882E